JOURNAL OF Applied Polymer SCIENCE

Rate-Dependent Self-Healing Behavior of an Ethylene-*co*-Methacrylic Acid Ionomer Under High-Energy Impact Conditions

Antonio Mattia Grande,[1] Luca Castelnovo,[1] Luca Di Landro,[1] Cinzia Giacomuzzo,[2] Alessandro Francesconi,[2] Mohammed Arifur Rahman[3]

[1]Dipartimento di Scienze e Tecnologie Aerospaziali, Politecnico di Milano, via La Masa 34, Milano 20156, Italy

[2]Dipartimento di Ingegneria Meccanica, Centro Interdipartimentale di Studi e Attività Spaziali CISAS "G. Colombo," Università di Padova, via Venezia 15, Padova 35131, Italy

[3]Dipartimento di Ingegneria Meccanica e Industriale, Università di Brescia, via Valotti 9, Brescia 25123, Italy

Correspondence to: A. M. Grande (E-mail: grande@aero.polimi.it)

ABSTRACT: In this work, the mechanical and the self-healing behaviors of an ethylene-*co*-methacrylic acid ionomer were investigated in different testing conditions. The self-healing capability was explored by ballistic impact tests at low-velocity, midvelocity, and hypervelocity bullet speed; different experimental conditions such as sample thickness and bullet diameter were examined; in all impact tests, spherical projectiles were used. These experiments, in particular those at low and midspeed, allowed to define a critical ratio between sample thickness and bullet diameter below which full repair was not observed. After ballistic damage, the healing efficiency was evaluated by applying a pressure gradient through tested samples. Subsequently, morphology analysis of the affected areas was made observing all tested samples by scanning electron microscope. This analysis revealed different characteristic features of the damaged zones affected at different projectile speed. Stress–strain curves in uniaxial tension performed at different temperatures and strain rates revealed yield strength and postyield behavior significantly affected by these two parameters. A rise of temperature during high strain rate tests in the viscoplastic deformation region was also detected. This behavior has a strong influence on the self-repairing mechanism exhibited by the studied material during high-energy impact tests. © 2013 Wiley Periodicals, Inc. J. Appl. Polym. Sci. 130: 1949–1958, 2013

KEYWORDS: properties and characterization; thermoplastics; mechanical properties; self-healing; ionomers

Received 14 February 2013; accepted 8 April 2013; Published online 10 May 2013

DOI: 10.1002/app.39384

INTRODUCTION

In recent years, one of the most attractive topics in material science is the study of self-healing materials. Many researchers are working on this matter and different approaches have been developed to obtain new polymeric materials with self-healing ability.[1–4] The repair strategies designed and yet developed can be mainly grouped into three major categories: repair by liquid healing agent incorporated in the material,[5,6] thermally induced repair carried out by a solid-phase material and intrinsic self-healing behavior exhibited by a number of polymers,[7,8] including ionomers.[9]

Ionomeric polymers, developed in the early 1960s, contain a certain percentage of ions (usually up to 20%) along the polymer chains.[10] They found significant applications in packaging and sport items (e.g., golf balls). Thanks to their self-healing behavior, they are currently considered also for applications in various fields of advanced engineering.

The self-healing behavior of these polymers after high-energy impact has been studied and described in several references.[11–13] The repair of damages is autonomous and instantaneous without any external intervention. The process can virtually be repeated many times, and this is a distinctive feature of these materials, especially when compared with other approaches that usually allow only a limited number of repeated repair cycles. Ionomers based on ethylene-*co*-methacrylic acid (EMAA) copolymer are one of the first class of polymeric materials which have been found to exhibit such self-healing behavior. In view of an extension of the properties range required in different potential applications, self-healing blends based on ionomers with the addition of different crystalline, elastomeric polymers, and modifiers have also been prepared and investigated.[14–18]

The self-repairing behavior following high-energy impact or puncture test, such as bullet penetration, was initially investigated by Kalista et al.[9,11] and Varley et al.[12,13] These studies were mainly focused on the self-healing behavior after ballistic

impacts and they investigated the effect of projectile shape and speed or environment conditions on the hole closure efficiency. Further researches followed thereby, to achieve a better understanding of the self-mending mechanism and new test methods were also developed.[19]

The self-healing phenomenon occurs spontaneously, without any external intervention, after impacts with energy high enough to allow the projectile to pass through the material in a very short time. The amount of energy transferred to the damaged material is thus believed as one of the main aspect influencing the healing capability, as it was well evidenced that the autonomic mending takes place only under defined conditions of temperature, speed and shape of the impacting object;[11–13] nonetheless, the exact relationship between the mechanical properties and the healing efficiency is still unclear. The use of EMAA-based polymers is currently limited to those events that pierce the material; however, researchers tried also to investigate the self-healing behavior of fiber reinforced composites by introducing thin layers of EMAA polymers in the stacking sequence.[20–23]

These materials have attracted researchers for their unusual mechanical properties. Akimoto et al.[24] studied the effect of aging conditions on mechanical behavior and proposed a model for the morphologic changes during material deformation; Scogna et al.[25,26] verified the applicability of Ree-Eyring model to the yielding of EMAA ionomers.

These materials are suitable for many potential applications, and it is therefore understandable the remarkable interest in the study of their repair process to develop new materials with similar ability over an extended range of conditions. Previous experimental activities have shown how different blends containing EMAA with about 30% of acid groups neutralized by Na ions and epoxidized natural rubber showed complete self-repairing phenomenon after ballistic impacts with pointed bullets.[16]

In this work, both mechanical and self-healing properties of EMAA ionomers with 30% of acid groups neutralized with sodium ions (EMAA-30Na) were evaluated through high-energy bullet impacts and tensile tests, studying the response of the material under different experimental conditions. The self-healing behavior after high-energy impact, the autonomic repair response of the ionomer has been studied by ballistic puncture tests under different conditions, which were assessed by varying sample thickness and projectile diameter; the same bullet shape was maintained: metallic spheres were launched in all performed tests. In view of possible applications such as in multilayer structures of space vehicles/stations or in antileakage protections for vehicle/aircraft fuel tanks, impact experiments were performed at low-velocity, midvelocity, and hypervelocity, thus extending the speed range investigated in previous studies.[11–13]

After all experiments, the healing efficiency was evaluated by applying a pressure gradient. Hole closure was tested both by following vacuum decay and by checking for possible flow of a fluid droplet placed at the damage zone with the applied pressure difference. A morphology analysis of the impact zones was also made observing all samples by scanning electron microscope (SEM) both in the bullet entrance and in the exit sides. The results showed a different behavior of the material subjected to impacts at different rates. At low bullet speed, a full melting process does not seem to take place; however, SEM analysis revealed small melted zones in the impact site. Furthermore, the self-healing behavior was detected up to a specific sample thickness/bullet diameter ratio (r/d). Similar results were obtained in tests at midbullet speed; in this case, an extension of the melted zone was also observed.

Conversely, in hypervelocity tests, a completely different morphology of the damaged areas was detected. Melting of the material in the impact zones occurred still maintaining in some condition an effective self-healing behavior. The promising self-healing response after hypervelocity impact tests suggests to consider the use of ionomers in multilayer composite materials for space applications such as inflatable structures.

Material heating during bullet puncture may be the result of different contributions such as strain energy dissipation, bullet friction and heat conduction from bullet to polymer. To get information about the relevance of thermal effects due to viscoplastic dissipation, tensile tests were performed at different strain rates and temperatures. In room temperature tests, samples were also observed with an IR camera to assess the variation of temperature during stretching. Even though strain rates employed in tensile tests were consistently lower than those experienced by the material during bullet impact a remarkable temperature increase was observed, which suggests a strong interdependence between thermal/mechanical behavior and healing capacity.

EXPERIMENTAL

Materials

Several grades of ionomers are commercially available, which differ in the percentage and kind of cations used for acid group neutralization (e.g., sodium, zinc, magnesium, and lithium). In this work, an ionomer based on EMAA copolymer, provided by DuPont® in pelletized form, was used (grade Surlyn® 8940). This ionomer is characterized by a content of 5.4 mol % acid groups, 30% of which neutralized with Na ions; its measured density and melting temperature are 0.95 g cm^{-3} and 94°C, respectively.

An hot press was used for the production of square plates (120 × 120 mm) with variable thickness from 0.5 up to 5 ± 0.2 mm; the temperature of the mold was set at 180°C and a molding pressure of 5 bars was used with a cooling rate of about 20°C min^{-1}; the pressure was maintained during cooling stage, until the removal of samples. Before production, the material was dried under vacuum at 60°C for 5 h.

Dog-bone specimens for tensile tests, according to ASTM D1708, were obtained from plates with 2 mm thickness. For bullet puncture tests, instead, square plates of different thickness were used. Before tensile and ballistic tests, the specimens were stored in a controlled environmental chamber at 23°C for 30 days to reach stable mechanical properties after aging.[26–28]

Ballistic Tests

Three different types of ballistic tests were carried out: the first test investigated self-healing ability of studied material after a low-velocity impact, while the second explored the ability to repair a damage following an impact at midvelocity. The last set of tests was aimed to study the self-healing response after impact at hypervelocity, a typical impact condition of the space environment consequent to the impact of micrometeoroids or debris.

The low-velocity tests were performed by shooting steel balls of different sizes using an air gun; this firing system allows to obtain a bullet velocity of about 180 ± 5 m s^{-1}. Actual bullet speed was measured using a Phantom v5.1 high-speed digital camera. Several tests were performed varying sphere diameter from 2.5 to 14.4 ± 0.15 mm and target samples thickness from 0.6 to 2.6 ± 0.2 mm.

Tests at midvelocity speed were carried out in a shooting lab; steel spheres with a diameter ranging from 1.5 to 7.5 ± 0.1 mm were fired with a shotgun, model Hatsan Optima, on samples with thickness of 0.5, 1, 2, and 3 ± 0.2 mm. The resulting speeds of spheres varied between 380 and 440 m s^{-1}. In this case, projectile velocity was measured using an optical chronograph, model CED M2 Millennium.

Hypervelocity impact tests were performed at CISAS - Hypervelocity Impact Facility at Padova University, using a two-stage Light-Gas Gun (LGG).[29] Velocities from 2 to 4 km s^{-1}, and target samples with thickness of 2, 3, and 5 ± 0.1 mm were explored. In this case, aluminum spheres with equal diameter of 1.5 mm were fired.

Healing Evaluation

The healing evaluation after ballistic tests was performed using two different techniques: microscopic observation and leakage test. The impact areas of all specimens were observed using an Hitachi, model TM-3000 SEM. Both bullet entrance and exit sides were analyzed to verify the hole closure and to evaluate the morphology of damaged surfaces. To better investigate the grade of healing, pressure leakage tests were also executed using a specific designed device developed for this purpose.[30] The close chamber of the experimental system was sealed with the sample and a pressure gradient of 0.9 bar was applied by a vacuum pump. When the hole was healed, no appreciable vacuum decay was detected compared to not punctured specimens during an observation time up to 15 min, while nonhealed samples showed a vacuum decay within few seconds.

Tensile Tests

Two different sets of tensile tests were performed. The first set investigated the rate dependency of stress-strain curves and the temperature rise in the material during uniaxial tensile tests. In these tests, force-displacement curves at 23°C were obtained with an MTS 858 testing system. Used crosshead speeds ranged from 0.1 to 500 mm s^{-1}, corresponding to strain rates from 4.5 × 10^{-3} to 22.7 s^{-1}. An infrared camera, Nikon S270 model, was used to monitor the temperature variation of the specimens during the experiments. The second set was aimed at verifying the dependence of mechanical properties both on temperature and strain rate. In this case, uniaxial tensile stress–strain curves in a temperatures range varying from −40 to 60°C were recorded with an Instron 4302, equipped with an Environmental Chamber 3119 including a liquid nitrogen cooling system. The crosshead speeds employed ranged from 10 to 500 mm min^{-1}, corresponding to strain rates from 7.5 × 10^{-3} to 3.8 × 10^{-1} s^{-1}. This second set of uniaxial tensile tests was also aimed at validating the Ree-Eyring model for yielding stress, extending previous results obtained by Scogna et al.[26]

RESULTS AND DISCUSSION

Ballistic Tests

Low-Velocity Impact Tests. The low-velocity impact tests, performed by firing steel spheres on EMAA-30Na plates, showed how this material is able to self-heal even under these experimental conditions. Tests were carried out varying the thickness of affected plates and the diameter of fired balls. The velocity of the spheres was set at 180 m s^{-1} for all performed tests. The healing was tested applying pressure difference in the damage zone and following vacuum decay. Sealed samples did not show an appreciable variation of pressure over time; otherwise, in the unrepaired specimens, vacuum decay was instantaneously recorded. These tests allowed to identify a critical ratio between sample thickness (t) and bullet diameter (d) below which full repair was not observed. This ratio is often recognized as a peculiar parameter to discriminate the impact behavior of flat panels.[31] Results presented in Table I show how above a 0.2 t/d ratio a complete self-healing behavior is well maintained; on the other hand, below this specific ratio, an effective hole closure did not occur. Pictures of a specimen entry side after low-velocity bullet impact are presented in Figure 1.

Table I. Low-Velocity Impact Test Results (No Self-Healing for Shaded Cells)

		Sphere diameter (mm)							
	t/d	2.35	3	5	6.34	8	10	12	14.27
Thickness (mm)	**0.6**	0.26	0.20	0.12	0.09	0.08	0.06	0.05	0.04
	1.0	0.43	0.33	0.20	0.16	0.13	0.10	0.08	0.07
	1.9	0.81	0.63	0.38	0.30	0.24	0.19	0.16	0.13
	2.6	1.11	0.87	0.52	0.41	0.33	0.26	0.22	0.18

t = sample thickness (mm), d = sphere diameter (mm).

Applied Polymer SCIENCE

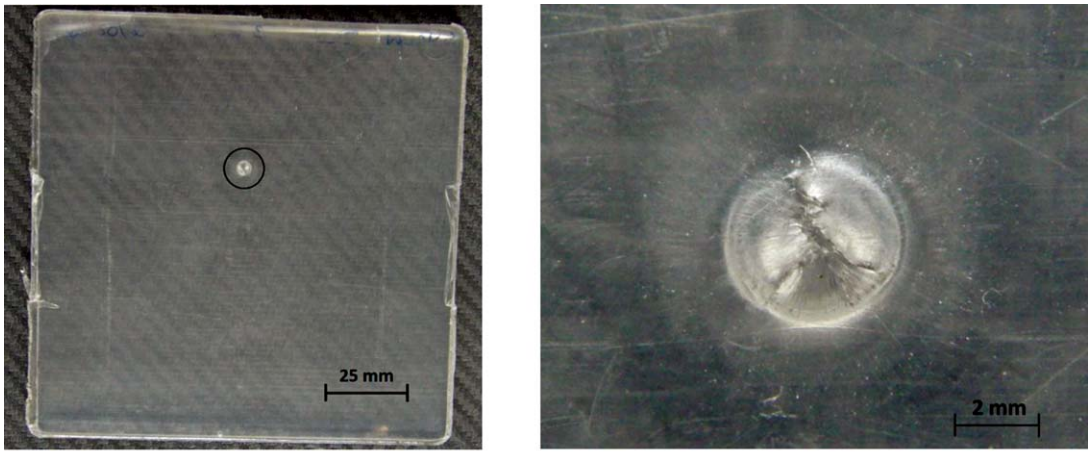

Figure 1. Images of the affected area (entry side) in a repaired sample, $t = 3$ mm, $d = 12$ mm tested at low velocity. [Color figure can be viewed in the online issue, which is available at wileyonlinelibrary.com.]

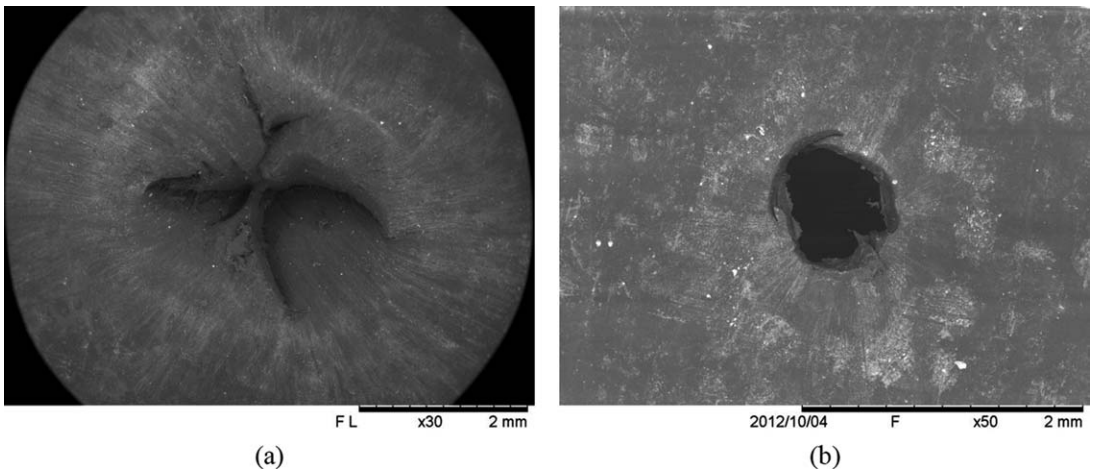

Figure 2. Entry side in a repaired sample (a), $t = 1.9$ mm, $d = 8$ mm, and unrepaired sample (b), $t = 0.6$ mm, $d = 3$ mm, tested at low velocity.

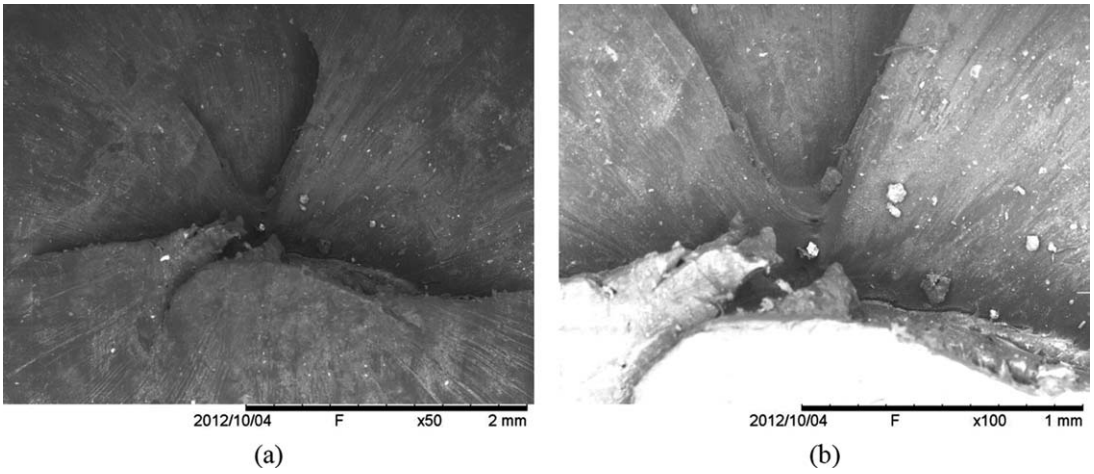

Figure 3. Entry side in a repaired sample, $t = 2.6$ mm, $d = 10$ mm, 50× magnification (a) and 100× magnification (b), tested at low velocity.

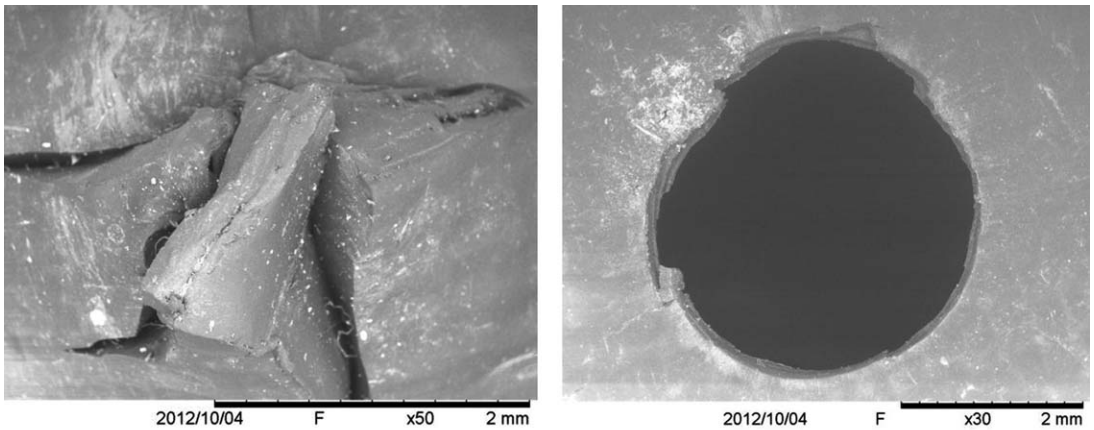

Figure 4. Exit side in a repaired sample (a), $t = 2.6$ mm, $d = 10$ mm, and unrepaired sample (b), $t = 1$ mm, $d = 5$ mm, tested at low velocity.

Table II. Midvelocity Impact Test Results (No or Partial Self-Healing for Shaded Cells)

		Sphere diameter (mm)						
	t/d	1.5	2.5	3.9	4.5	6.2	7.5	
Thickness (mm)	**0.5**	0.33	0.20	0.13	0.11	0.08	0.07	No SH
	1.0	0.67	0.40	0.26	0.22	0.16	0.13	50% SH
	2.0	1.33	0.80	0.51	0.44	0.32	0.27	
	3.0	2.00	1.20	0.77	0.67	0.48	0.40	

t = sample thickness (mm), d = sphere diameter (mm).

Microscope analysis after low-velocity ballistic tests highlighted different morphologies of the affected areas compared with those previously obtained in other studies; however, some similarities can be still recognized. In the bullet entry side (Figure 2), it is possible to see radial striations in the direction of the impact point caused by plastic deformation both in healed and no healed samples. However, a significant difference in the response of the material after impact was detected; the morphology of the damaged area in healed samples presented petaling phenomenon [Figures 2(a) and 3(a)] with a melted zones on the apex of the petals [Figure 3(b)]. These melted areas, even if small, are responsible for the sealing of the hole caused by the bullet, thus becoming a crucial factor for the global self-healing behavior exhibited by the studied material. On the other hand, nonhealed samples present a circular hole with clearly defined edges [Figure 2(b)], which evidence removal of material preventing the repair. Regarding the exit side, healed samples show the same

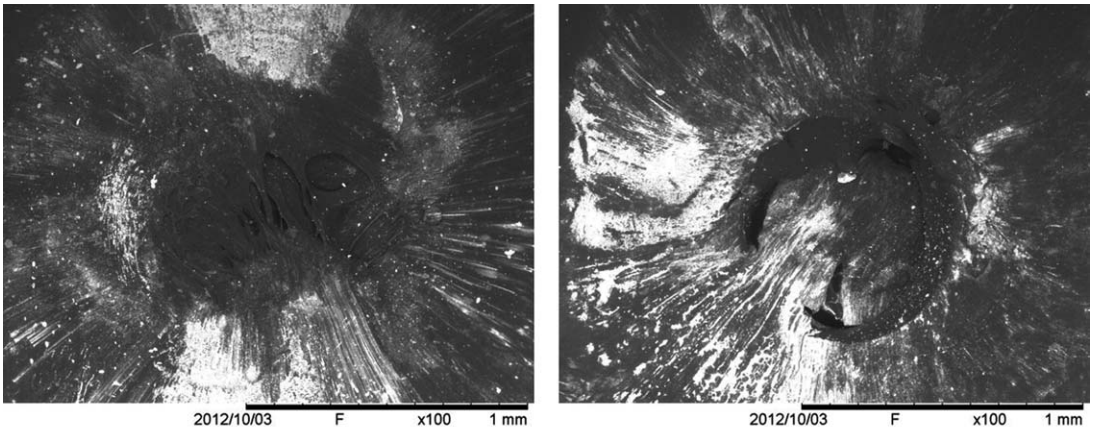

Figure 5. Entry side in a repaired sample (a), $t = 1$ mm, $d = 1.5$ mm, and unrepaired sample (b), $t = 0.5$ mm, $d = 1.5$ mm, tested at midvelocity.

Applied Polymer SCIENCE

Table III. Hypervelocity Impact Test Results

Diameter (mm)	Velocity (km s^{-1})	Thickness (mm)	t/d	Healing (hole closure)	Healing (leakage test)
1.5	1.93	2	1.33	Yes	Yes
1.5	1.80	3	2.00	Yes	No
1.5	1.64	5	3.33	Yes	Yes
1.5	3.90	2	1.33	No	No
1.5	4.00	3	2.00	Yes	Yes
1.5	4.10	5	3.33	Yes	Yes

petal morphology although a clear melted zone is not detectable [Figure 4(a)]: this behavior suggests that in the entry side, an additional contribution to temperature increment may derive from the friction forces between bullet and impact surface; such friction is expected to be lower in the exit side as consequence of material deformation. Unrepaired samples present instead a morphology quite similar to that presented in the entry side [Figure 4(b)].

Midvelocity Impact Tests. In these tests, as in the previous case, steel spheres of different diameter were fired on square samples with thickness varying between 0.5 and 3 ± 0.2 mm; results of midvelocity impact tests are presented in Table II. Also at this impact speed, a critical t/d ratio, between 0.3 and 0.4, can be valued, below which self-healing behavior did not appear. In few cases, a clear distinction between complete or partial hole closure is not possible: about the 50% of thin samples (0.5 mm) fired with 1.5 and 2.5 show an effective repair.

For repaired samples, SEM analysis revealed a morphology of the impact sites with a clear melted zone in the center of the crater and radial striations due to extensive deformation [Figure 5(a)]. On the other hand, unrepaired sample present clear-cut holes similar to those obtained after low-velocity impacts. However, in some cases, a competition between these two failure modes occurred. In Figure 5(b), both a clear break and a melted zone still attached to the material removed by the projectile impact can be observed.

Hypervelocity Impact Tests. Impact experiments performed at hypervelocity with 1.5-mm-diameter spheres prove the healing behavior of EMAA-30Na at the two tested speed ranges, that is, 2 and 4 km s^{-1}; results are summarized in Table III. At the

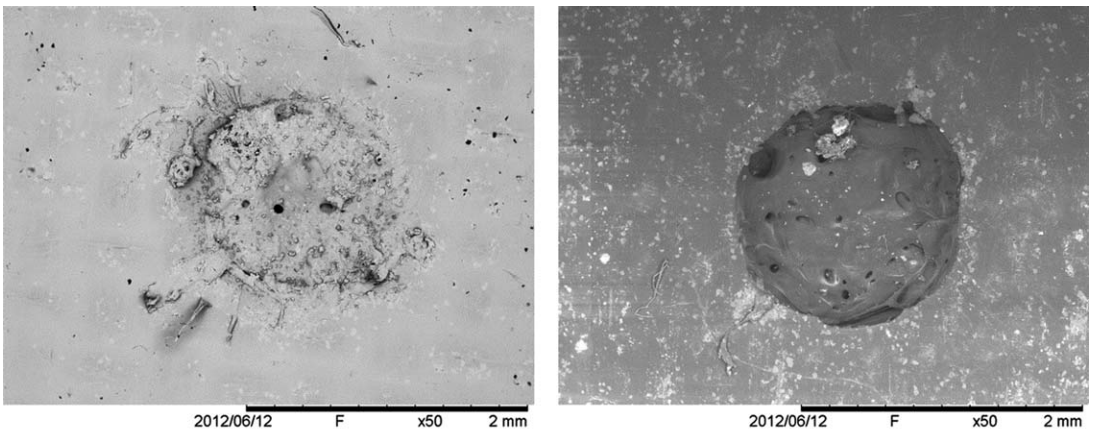

Figure 6. Sample of 2 mm thickness tested at 2 km s^{-1}: entry side (a) and exit side (b).

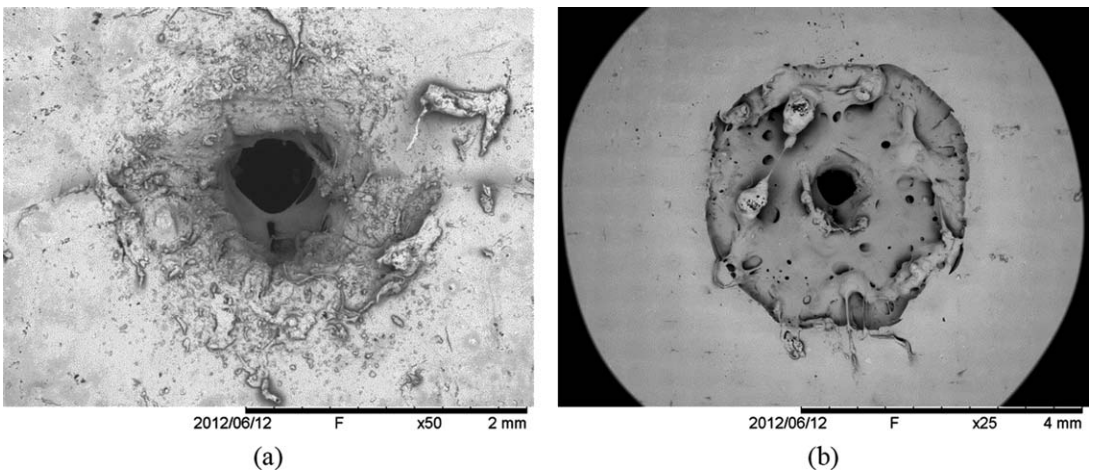

Figure 7. Sample of 2 mm thickness tested at 4 km s^{-1}: entry side (a) and exit side (b).

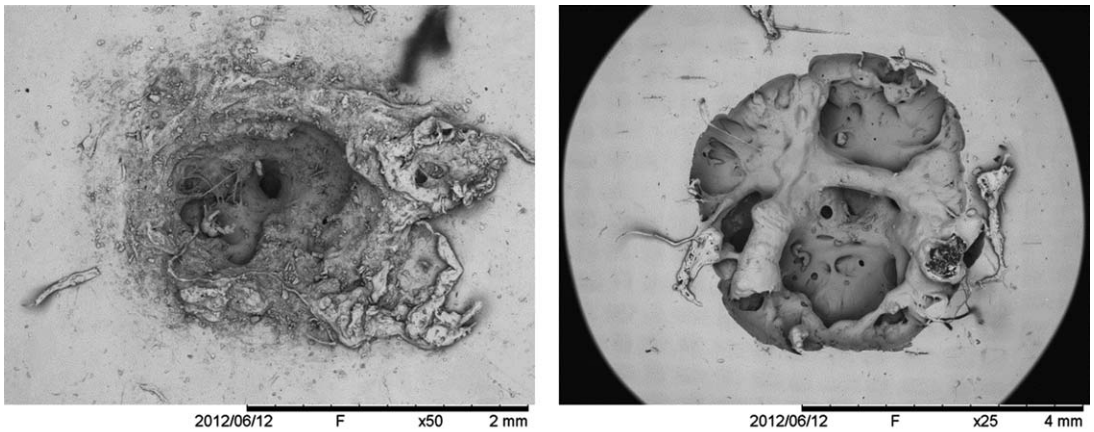

Figure 8. Sample of 3 mm thickness tested at 4 km s^{-1}: entry side (a) and exit side (b).

lowest projectile velocity, 2 km s^{-1}, all ionomeric samples visually exhibited complete hole closure, but leakage tests showed a loss of pressure of the 3-mm-thick specimen. Conversely, at the highest bullet speed, 4 km s^{-1}, only the 3- and 5-mm-thick samples exhibited complete hole closure.

Morphological analysis after hypervelocity tests showed a completely different conformation of the affected sites from those previously analyzed; some differences were also detected among the various tested samples. In all tested plates, on the inlet side, debris of the fired aluminum sphere can be observed; nevertheless, on the other side, no residues of the projectile were detected (Figures 6–9).

Samples of 2 mm thickness affected at 2 km s^{-1} and samples of 2 and 3 mm thickness affected at the highest speed presented the same morphology of the damaged area. The bullet entry zones show an indented surface [Figures 6(a), 7(a), and 8(a)]; on the other hand, the morphology of the impact area on the back part of these samples exhibit a clearly defined melted zone of approximately the same diameter as spherical projectile in the first case [Figure 6(b)] and of about 4 mm in the second case [Figures 7(b) and 8(b)]. In addition, the presence of voids caused probably by the generation of volatile substances during the impact can be inferred from observations. All other tested samples show an impact crater with similar characteristics both in the entry and exit sides. As presented in Figure 9, in each side a melted zone can be observed together with some filaments of flowed polymer starting from the impact site.

Tensile Tests

Tensile tests of ionomeric samples were performed at different temperatures and strain rates. The first set of tests was performed at room temperature and at varying strain rate. An IR camera was also used to measure temperature variations of tested samples during stretching. Obtained results revealed a marked dependence of the mechanical behavior of studied material on strain rate; in particular, an increase in the deformation rate gives an increase in the instantaneous Young modulus, yield, and postyield stress level. A decrease of strain at break was, instead, detected.

In specimens stretched to highest strain rate, a remarkable heating effect due to the dissipated deformation energy was detected, with increase of temperature up to 32°C. All specimen

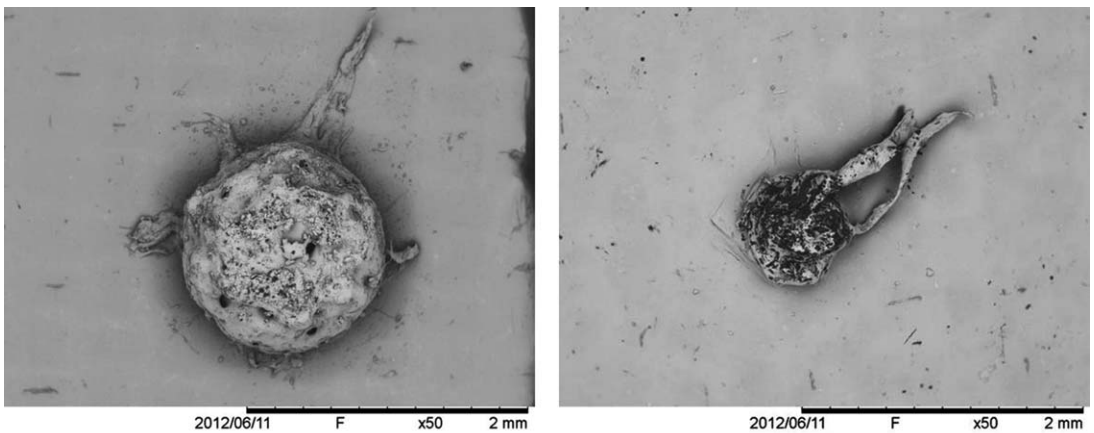

Figure 9. Sample of 3 mm thickness tested at 2 km s^{-1}: entry side (a) and exit side (b).

Applied Polymer SCIENCE

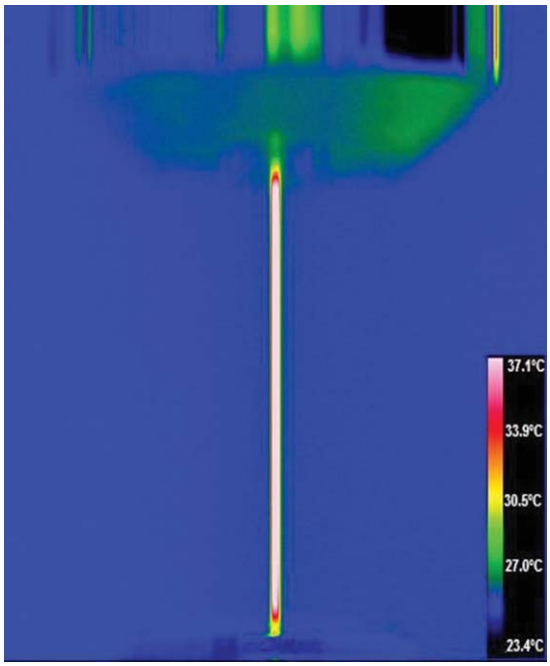

Figure 10. IR camera frame during tensile test. [Color figure can be viewed in the online issue, which is available at wileyonlinelibrary.com.]

presented extensive plastic deformation with strain at break always exceeding 190%. Observing specimens through IR camera during tensile tests (Figure 10), it seems that the temperature is homogenous throughout samples suggesting an equally homogenously distributed plastic deformation. In Figure 11, the evolution of temperature in tested samples at the different strain rate is presented; in the same figure, the resulting stress–strain curves are superposed. It can be observed that on increasing strain rate and corresponding temperature the "strain hardening" progressively reduces; a thermal softening effect is apparent. However, it is expected that specimen temperature is affected by heat transmission from the sample to the external environment by convection and conduction, which cannot be avoided.

To study in depth the yielding and breaking behavior of the material, tensile tests at different temperature and different, but

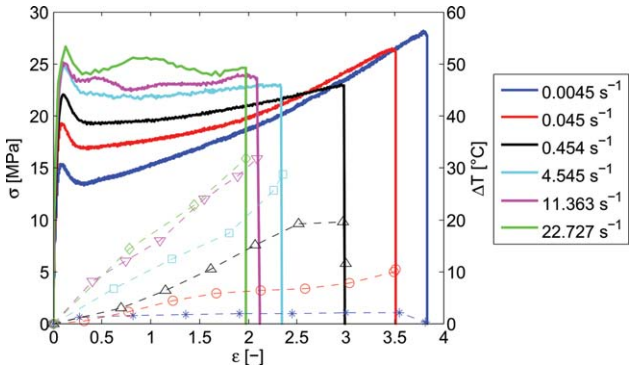

Figure 11. Temperature rise superposed on stress–strain curve for tensile test at different strain rates at room temperature. [Color figure can be viewed in the online issue, which is available at wileyonlinelibrary.com.]

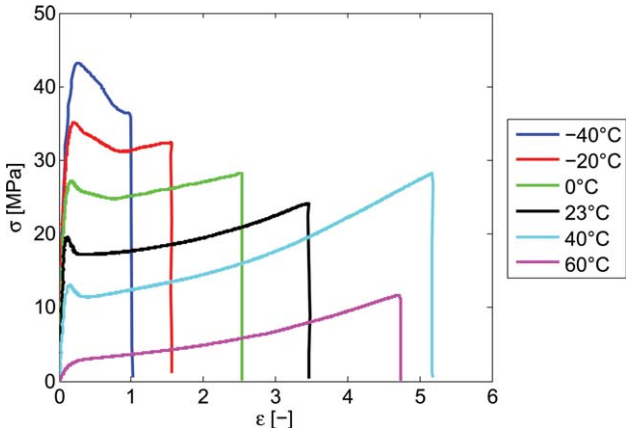

Figure 12. Stress–strain curves at different temperature at strain rate of 0.136 s^{-1}. [Color figure can be viewed in the online issue, which is available at wileyonlinelibrary.com.]

lower, strain rates were also performed. In these experiments, the actual temperature of the sample can be considered equal to the one set in the environmental chamber due to low applied strain rates. An example of the temperature dependence of stress–strain curves at a strain rate of 0.136 s^{-1} is reported in Figure 12. As expected, mechanical properties such as the instantaneous Young modulus and the yield stress, decrease with increasing temperature. A change in the fracture behavior was also noticed during the tests: at −40°C, an abrupt break occurs immediately after necking, while at higher temperatures, consistent flow takes place, and a viscoplastic behavior is promoted. An interesting observation is that the increase of temperature from −40°C leads to a continuous increase of the ultimate deformation and reduction of ultimate stress up to 40°C. At 60°C, the opposite trend was observed and a change in morphology underlined by the whitening of the specimen (Figure 13) was evidenced; an easier strain-induced crystallization process due to stretching and chains alignment probably occurred. Moreover, at this temperature, a peak stress at yielding point is not

Figure 13. Evolution of type of fracture with temperature: untested sample (a), −40°C (b), −20°C (c), 0°C (d), 23°C (e), 40°C (f), and 60°C (g). [Color figure can be viewed in the online issue, which is available at wileyonlinelibrary.com.]

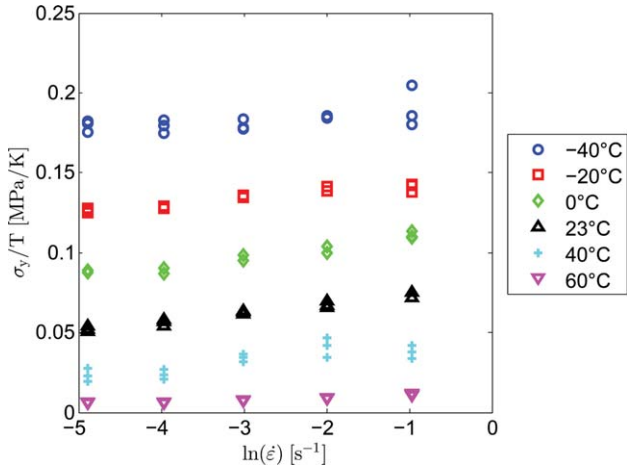

Figure 14. Measured yield stress at various strain rates and the temperatures. [Color figure can be viewed in the online issue, which is available at wileyonlinelibrary.com.]

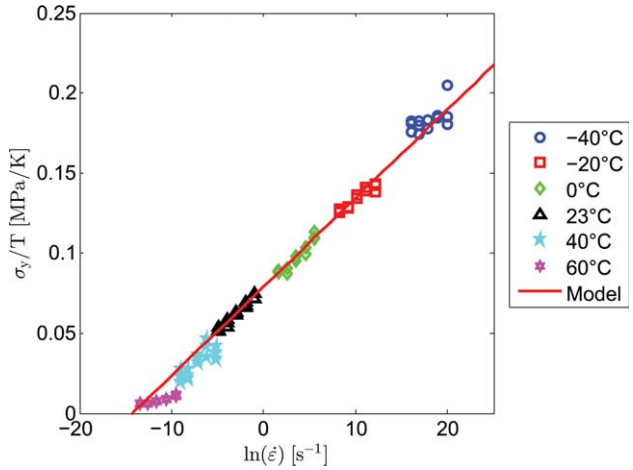

Figure 15. Obtained master curve at T_{ref} = 23°C. [Color figure can be viewed in the online issue, which is available at wileyonlinelibrary.com.]

so evident as at lower temperatures because the transition related to the melting of secondary crystals has already happened and aging effects were not presented.[26–28]

The yield stress values resulting from this last set of tests performed at different temperatures and strain rates were determined as the local maximum of stress–strain curves; results are shown in Figure 14. Assuming that a single relaxation process is involved, the yield stress was modeled with the Ree-Eyring equation:

$$\frac{\sigma_y}{T} = \frac{R}{v}\sinh^{-1}\left[\frac{\dot{\varepsilon}}{\dot{\varepsilon}_0}\exp\left(\frac{\Delta H}{RT}\right)\right] \quad (1)$$

where R is the gas constant, v is the activation volume, $\dot{\varepsilon}$ is the applied strain rate, $\dot{\varepsilon}_0$ is a constant pre-exponential factor, ΔH is the activation energy, and T the absolute temperature. The results achieved by fitting the measured yield stress at different strain rates and temperatures with Ree-Eyring model are summarized in Table IV. Exploiting the superposition principle is also possible to build a master curve which, selecting a reference temperature, describes the yield stress of the studied material over a wide range of strain rates; in particular the tests at lower temperature give an insight on the response of the material at higher strain rates, characteristic of ballistic impacts.

Datasets taken at various temperatures were superimposed to create the master curve at the reference temperature (T_{ref}=23°C). The horizontal shift factors, s_x, are given by an Arrhenius expression:

$$s_x = -\frac{\Delta H}{R}\left(\frac{1}{T_{ref}} - \frac{1}{T}\right) \quad (2)$$

with activation energy ΔH obtained for the Ree-Eyring process.

Table IV. Ree-Eyring Model Fit Parameters

v(nm^3)	ΔH(kJ mol^{-1})	$\dot{\varepsilon}_0$ (s^{-1})
5.00	190.16	2.28×10^{27}

The master curve at the reference temperature is shown in Figure 15.

These results show how the stress–strain behavior of studied material is deeply dependent on strain rate and temperature showing also a coupling between mechanical and thermal response when subjected to large deformations. Definitely, these inter-relations may play an important role in the self-healing behavior after ballistic impact of studied material; further analysis can give the necessary insight for a complete understanding of this phenomenon.

CONCLUSIONS

Self-healing behavior after ballistic puncture tests and mechanical properties of EMAA-30Na ionomer were investigated under different experimental conditions. Impact tests were carried out firing spherical projectiles at different speeds ranging from low, 180 m s^{-1}, up to hypervelocity, 4 km s^{-1}. After ballistic tests, healing efficiency was checked by SEM micrographs and air leakage tests.

Apparently, at low-velocity impact tests, a clear melted zone is not detectable in both sides; however, a more extensive microscopic analysis clarified the presence of small melted areas in bullet entry sides. An increase of temperature due to the plastic deformation and to bullet friction can be assumed according to the results obtained in mechanical tests. This rise in temperature during the bullet passage promoted the repair even for these low speed impacts allowing the hole sealing immediately after the elastic recovery. A critical t/d ratio of 0.2 for low-velocity impact tests was found.

Midvelocity impact tests revealed instead a competition between two different failure behaviors; still, a critical t/d relationship was evidenced. Also in this case, the melting of the polymer in the area of impact plays an important role for the complete hole closure after projectile passage.

Moreover, hypervelocity tests showed the ability of studied material to self-heal even under these severe test conditions suggesting a possible use of EMAA-30Na in the space field.

Microscope analyses after impact detected a complete different morphology of the damaged areas not comparable with the previous cases.

Mechanical tests and temperature recordings showed how the heat generated by plastic deformation may consistently give a fundamental contribution to the sealing of the hole after high-energy impacts. Tensile tests performed at different strain rates allowed to evidence and measure the increment of temperature of specimens during the experiments.

ACKNOWLEDGMENTS

The sponsorship of Regione Lombardia—projects STIMA and SMAT—is gratefully acknowledged. The authors thank the company DuPont (Italy) for providing the ionomeric material.

REFERENCES

1. Van der Zwaag, S.; van Dijk, N. H.; Jonkers, H. M.; Mookhoek, S. D.; Sloof, W. G. *Philos. Trans. R. Soc. A* **2009**, *367*, 1689.
2. Blaiszik, B. J.; Kramer, S. L. B.; Olugebefola, S. C.; Moore, J. S.; Sottos, N. R.; White, S. R. *Annu. Rev. Mater. Res.* **2010**, *40*, 179.
3. Wu, D. Y.; Meure, S.; Solomon, D. *Prog. Polym. Sci.* **2008**, *33*, 479.
4. Murphy, E. B.; Wudl, F. *Prog. Polym. Sci.* **2010**, *35*, 223.
5. White, S. R.; Sottos, N. R.; Geubelle, P. H.; Moore, J. S.; Kessler, M. R.; Sriram, S. R.; Brown, E. N.; Viswanathan, S. *Nature* **2001**, *409*, 794.
6. Pang, J. W. C.; Bond, I. P. *Compos. A* **2005**, *36*, 183.
7. Chen, X.; Dam, M. A.; Ono, K.; Mal, A.; Shen, H. B.; Nutt, S. R.; Sheran, K.; Wudl, F. *Science* **2002**, *295*, 1698.
8. Cordier, P.; Tournilhac, F.; Soulie-Ziakovic, C.; Leibler, L. *Nature* **2008**, *451*, 977.
9. Kalista, S. J.; Ward, T. C.; Oyetunji, Z. *Mech. Adv. Mater. Struct.* **2007**, *14*, 391.
10. Holiday, L. Ionic Polymer; Applied Science: London, **1975**.
11. Kalista, S. J.; Ward, T. C. *J. R. Soc. Interface* **2007**, *4*, 405.
12. Varley, R. J.; van der Zwaag, S. *Acta Mater.* **2008**, *56*, 5737.
13. Varley, R. J.; van der Zwaag, S. *Polym. Int.* **2010**, *59*, 1031.
14. Penco, M.; Rahman, M. A.; Spagnoli, G.; Janszen, G.; Di Landro, L. *Mater. Lett.* **2011**, *65*, 2107.
15. Rahman, M. A.; Penco, M.; Spagnoli, G.; Grande, A. M.; Di Landro, L. *Macromol. Mater. Eng.* **2011**, *296*, 1119.
16. Rahman, M. A.; Penco, M.; Peroni, I.; Ramorino, G.; Grande, A. M.; Di Landro, L. *ACS Appl. Mater. Interfaces* **2011**, *3*, 4865.
17. Rahman, M. A.; Spagnoli, G.; Grande, A. M.; Di Landro, L. *Macromol. Mater. Eng.* **2013**, doi:10.1002/mame.201200399, In press. http://onlinelibrary.wiley.com/doi/10.1002/mame.201200399/abstract.
18. Varley, R. J.; Shen, S.; van der Zwaag, S. *Polymer* **2010**, *51*, 679.
19. Varley, R. J.; van der Zwaag, S. *Polym. Test.* **2008**, *27*, 11.
20. Meure, S.; Varley, R. J.; Wu, D. Y.; Mayo, S.; Nairn, K.; Furman, S. *Eur. Polym. J.* **2012**, *48*, 524.
21. Pingkarawat, K.; Wang, C. H.; Varley, R. J.; Mouritz, A. P. *Compos. A* **2012**, *43*, 1301.
22. Pingkarawat, K.; Wang, C. H.; Varley, R. J.; Mouritz, A. P. *J. Mater. Sci.* **2012**, *47*, 4449.
23. Varley, R. J.; Parn, G. P. *Compos. Sci. Technol.* **2012**, *72*, 453.
24. Akimoto, H.; Kanazawa, T.; Yamada, M.; Matsuda, S.; Shonaike, G. O.; Murakami, A. *J. Appl. Polym. Sci.* **2001**, *81*, 1712.
25. Scogna, R. C.; Register, R. A. *J. Polym. Sci. Part B* **2009**, *47*, 1588.
26. Scogna, R. C.; Register, R. A. *Polymer* **2009**, *50*, 585.
27. Kulkarni, H. P.; Mogilevsky, G.; Mullins, W. M.; Wu, Y. *J. Mater. Res.* **2009**, *24*, 1087.
28. Loo, Y.; Wakabayashi, K.; Huang, Y. E.; Register, R. A.; Hsiao, B. S. *Polymer* **2005**, *46*, 5118.
29. Angrilli, F.; Pavarin, D.; De Cecco, M.; Francesconi, A. *Acta Astronaut.* **2003**, *53*, 185.
30. Grande, A. M.; Coppi, S.; Di Landro, L.; Sala, G.; Giacomuzzo, C.; Francesconi, A.; Rahman, M. A. *Proc. SPIE* **2012**, 8342.
31. Francesconi, A.; Giacomuzzo, C.; Grande, A. M.; Mudric, T.; Zaccariotto, M.; Etemadi, E.; Di Landro, L.; Galvanetto, U. *Adv. Space Res.* **2013**, *51*, 930.